Frontiers in Bioscience Landmark

Front. Biosci. (Landmark Ed) **2025**; 30(12): 47450
https://doi.org/10.31083/FBL47450

Original Research

Single-Cell Dissection of Fibroblast Heterogeneity in Diabetic Ulcers: Platelet-Rich Plasma (PRP) Therapy Activates Core Regenerative Programs via PLAGL1/RUNX2/ZKSCAN7 Networks

Xiongjie Li[1,†], Zhenghao He[1,†], Chenyan Long[1,2], Manli Chen[1], Lizhen Zhang[1], Zhijun Luo[1], Ju Tian[1,3,*]

[1]Department of Burns and Plastic Surgery, Zhongshan City People's Hospital, 528400 Zhongshan, Guangdong, China
[2]Department of Burns and Plastic Surgery, Shantou City People's Hospital, 515000 Shantou, Guangdong, China
[3]Department of Plastic Surgery, Affiliated Hospital of Guangdong Medical University, 524000 Zhanjiang, Guangdong, China
*Correspondence: tian-ju@163.com (Ju Tian)
[†]These authors contributed equally.

Academic Editor: Pietro Gentile
Submitted: 17 October 2025 Revised: 19 November 2025 Accepted: 25 November 2025 Published: 18 December 2025

Abstract

Objective: This integrated study aimed to characterize fibroblast heterogeneity in diabetic ulcers and evaluate the efficacy of platelet-rich plasma (PRP) using multi-omics approaches. **Methods**: We analyzed single-cell RNA sequencing (scRNA-seq) data (GSE165816) from healed (n = 9) and non-healed (n = 5) patients with diabetic foot ulcers (DFU) to characterize fibroblast dynamics, utilizing cell–cell communication analysis, transcription factor profiling, and pseudotime trajectory reconstruction. A streptozotocin-induced diabetic ulcer rat model was established to validate the therapeutic effects of PRP. **Results**: scRNA-seq identified 13 cell types, with fibroblasts showing the most significant proportional increase in healed DFU (32% versus 25% in non-healed tissue). Fibroblast-centric communication networks revealed synergistic interactions with endothelial and keratinocyte lineages. Three key transcription factors (PLAGL1, RUNX2, and ZKSCAN7) were upregulated in healed fibroblasts, regulating pathways related to extracellular matrix (ECM) synthesis, angiogenesis, and cell migration. Pseudotemporal analysis confirmed the differentiation of fibroblasts toward ECM-producing states, with enrichment of platelet-derived growth factor (PDGF) signaling pathways. In the rat model, PRP treatment resulted in epidermal/dermal thickening, reduced inflammatory infiltration, and transcriptomic reprogramming that converged with non-diabetic profiles. Venn analysis identified a 26-core gene signature (e.g., *COL1A1*, *FN1*) associated with fibroblast-mediated ECM reorganization. **Conclusion**: Fibroblasts drive diabetic ulcer healing *via* transcription factor-regulated functional networks. PRP accelerates tissue repair by modulating fibroblast ECM-related gene expression, with the 26-gene signature providing a promising foundation for novel diagnostic and therapeutic targets.

Keywords: diabetic foot; wound healing; fibroblasts; platelet-rich plasma; single-cell analysis; RNA sequencing; transcription factors; extracellular matrix

1. Introduction

Diabetes represents a major global health challenge, with its complications profoundly reducing patients' quality of life and imposing a substantial burden on healthcare systems [1]. Among these complications, diabetic ulcers, particularly Diabetic Foot Ulcers (DFU), are among the most difficult to manage; these chronic, lower-extremity wounds often fail to respond to conventional therapies [2]. DFUs markedly increase hospitalization and amputation rates and are a major contributor to the elevated mortality observed in diabetic populations [2,3]. Despite advances in overall diabetes management, effective treatment of DFU remains a pressing and unresolved clinical challenge [4]. Fibroblasts are essential mediators of wound repair, secreting extracellular matrix (ECM) components and cytokines that drive tissue reconstruction [5,6]. However, under diabetic conditions, fibroblast function becomes markedly impaired, resulting in delayed or incomplete wound closure [7]. The advent of single-cell RNA sequencing (scRNA-seq) has transformed the study of complex tissue microenvironments by enabling high-resolution analysis of cellular heterogeneity and functional states [8]. This technology provides unprecedented insight into fibroblast subpopulations within DFU and allows their dynamic behaviors during wound healing to be characterized at single-cell resolution [9].

Platelet-rich plasma (PRP), an autologous blood product enriched with growth factors and cytokines, has been shown to promote tissue repair and regeneration [10,11]. Growing evidence suggests that PRP holds substantial therapeutic potential for the treatment of chronic wounds [12, 13]. However, the precise mechanisms through which PRP facilitates healing in diabetic ulcers remain incompletely understood. In particular, how PRP modulates fibroblast function, a central driver of wound repair, requires further clarification.

This study analyzed single-cell RNA sequencing data (GSE165816) from the GEO database to compare fibroblast heterogeneity and functional states between DFU-healer and DFU-nonhealer patients. In parallel, we evaluated the therapeutic effects of PRP on fibroblast activity and ulcer repair using a diabetic ulcer rat model. By integrating cell–cell communication analysis, transcription factor profiling, and protein interaction network mapping, we elucidated the functional roles of fibroblasts in diabetic ulcers healing and investigated the molecular mechanisms through which PRP may exert its therapeutic benefits. These findings provide new insights into fibroblast-driven wound repair and offer a theoretical basis for improving diabetic ulcers management.

2. Materials and Methods

2.1 Data Sources and Download

The single-cell RNA sequencing dataset used in this study was obtained from the GEO database (accession number GSE165816) [14]. A total of nine DFU-healer samples and five DFU-nonhealer samples were included for downstream analyses.

2.2 Single-Cell Sequencing Data Processing

Single-cell data were initially processed using the Seurat package (version 5.2.1), and batch effects were mitigated using the Harmony package [15,16]. The dataset was constructed with ingestion-level filtering via the CreateSeuratObject function (min.features = 300, min.cells = 5). To ensure analytical transparency without modifying the original clustering or t-SNE visualizations, a quality-control audit was performed on the final analysis object. Mitochondrial gene content (percent.mt) for each cell was calculated using the human mitochondrial gene prefix (^MT-), and sample-level median percent.mt values are reported in the Results section. Doublet prediction was conducted using DoubletFinder (Seurat v5 interface; version 2.0.6) with PCs 1–30, pN = 0.25, and expected doublet counts adjusted using the modelHomotypic function in a two-step pANN reuse workflow. Predicted doublet rates were documented, but no cells were removed to preserve the original clustering structure and figures. Batch correction was performed with Harmony (version 1.2.0) using the first 30 principal components (PCs), selected based on: (i) an elbow inflection around PCs 28–32; (ii) JackStraw significance across the first ~30 PCs; and (iii) stability of clustering and neighborhood topology under PC = 20, 30, or 40, with no change in biological interpretation. As all original figures were generated using t-SNE, this visualization method was retained post-Harmony for consistency and for its clear delineation of fibroblast subclusters. UMAP was evaluated internally and produced comparable biological conclusions. Differential expression (DE) analyses were performed in Seurat using FindMarkers and FindAllMarkers with the two-sided Wilcoxon rank-sum test on log-normalized expression values. Multiple testing correction was applied using the Benjamini–Hochberg method, and genes were defined as significantly differentially expressed when they met an adjusted p value (FDR) <0.05 and an absolute $\log_2$ fold-change >0.25. For each comparison, we report the gene symbol, $\log_2$ fold-change, adjusted p value, and the percentage of cells expressing the gene in each group.

2.3 Cell-Type Annotation and Marker Discovery

Cell-type annotation was performed by integrating canonical lineage markers, cluster-level differential expression patterns, and reference information from the published DFU atlas (GSE165816) by Theocharidis [14]. Consistent with this reference, fibroblasts were identified using DCN as a canonical dermal fibroblast marker, while CFD was retained as a marker enriched in reticular/adipogenic-like fibroblast subtypes, thereby preserving comparability with the source dataset. To ensure transparency in cluster assignment, we computed cluster-specific marker genes using Seurat:FindAllMarkers (only.pos = TRUE, min.pct = 0.10, logfc.threshold = 0.25; Wilcoxon test; Benjamini–Hochberg correction). For each cluster, the top 20 upregulated markers, reported with avg_$\log_2$FC, adjusted p value, pct_in_cluster, and pct_other, are provided in **Supplementary Table 1**.

2.4 Cell Communication and Transcription Factor Analysis

Intercellular communication networks were analyzed using the iTALK package (https://github.com/Coolgenome/iTALK), which incorporates a curated ligand–receptor database to identify and match signaling pairs. Transcription factor activity was assessed with the SCENIC package (version 1.3.1), which reconstructs gene regulatory networks and cellular states through integrated co-expression and DNA motif analyses [17]. Co-expression networks were first inferred using GRNBoost, after which motif enrichment and target gene prediction were performed with RcisTarget. Regulatory network activity was quantified using the AUCell algorithm, enabling identification of transcription factors and their target genes with cell type–specific enrichment.

2.5 Analysis of Fibroblasts

Following the extraction of all fibroblasts, dimensionality reduction was performed, and differentially expressed genes (DEGs) between DFU-healer and DFU-nonhealer fibroblasts were identified using the *FindMarkers* function in Seurat. Consistent with the global analysis workflow, DEGs were defined using the Wilcoxon rank-sum test with Benjamini–Hochberg correction (FDR <0.05 and $|\log_2 FC| > 0.25$). Gene enrichment analyses were conducted using the cluster Profiler package (version 4.9.0.2) [18]. Pseudotime trajectory reconstruction was carried out using the Monocle package (version 2.24.0) with default parameters,

applying the DDRTree algorithm for dimensionality reduction and temporal cell ordering [19]. Pseudotime was computed exclusively within fibroblasts to avoid cross–cell-type mixing. After Seurat log-normalization (scale factor 10,000) and selection of 2000 highly variable genes (VST method), count matrices were imported into Monocle2 (version 2.24.0; expressionFamily = negbinomial.size). Size factors and dispersions were estimated, dimensionality reduction was performed using DDRTree (max_components = 2), and cells were ordered along inferred trajectories using orderCells. The root state was defined a priori as the homeostatic/quiescent fibroblast subset, characterized by high *DCN*, *COL1A1/COL1A2*, and *PDGFRA* expression and low *ACTA2* and *TAGLN* expression, located at a terminal tip of the learned trajectory graph. Branch expression analysis modeling was subsequently performed to characterize cell fate decisions along divergent pseudotime branches.

2.6 Protein Interaction Analysis

Protein interaction networks were constructed using the STRING database (version 12.0), which provides a comprehensive repository encompassing 12,535 organisms, 59.3 million proteins, and more than 20 billion experimentally supported interactions. Significant functional interaction modules were subsequently identified using the MCODE plugin within Cytoscape 3.8.0 (The Cytoscape Consortium, Seattle, WA, USA). The MCODE algorithm was applied with the following parameters: Node Score Cutoff = 0.2, K-Core = 2, and Max Depth = 100.

2.7 Establishment of a Diabetic Ulcer Rat Model

Diabetes was induced in the experimental rats by intraperitoneal injection of streptozotocin (STZ) [20]. Prior to injection, rats were fasted but allowed free access to water. STZ was dissolved in sterile saline at a concentration of 30 mg/mL and administered at a dosage of 30 mg/kg. After 72 hours, blood samples were collected from the tail vein to confirm successful diabetes induction, defined as a blood glucose level $>$16.7 mmol/L. Eight weeks after diabetes induction, rats were anesthetized with isoflurane. Anesthesia was initiated by exposing animals to 2% (v/v) isoflurane delivered at a flow rate of 3 mL/min for approximately 10 minutes. A third-degree burn wound was then generated on the dorsal surface by applying a red-hot circular iron for 30 seconds. To prevent wound contraction, a hard plastic ring was surgically secured around the injury site and covered with sterile gauze. Any emerging epithelial tissue was removed regularly to maintain the wound in an unhealed state for one month.

2.8 Preparation of Platelet-Rich Plasma

Blood was collected into EDTA-K2 vacuum tubes and gently inverted to prevent clotting or hemolysis. A 1-mL aliquot was withdrawn for complete blood count analysis. PRP was prepared using a two-step centrifugation protocol: an initial centrifugation at 900 *g* for 5 minutes, followed by a second centrifugation at 1500 *g* for 15 minutes. After the second spin, the supernatant was collected as platelet-poor plasma (PPP), while the remaining platelet pellet was resuspended to generate PRP. Platelet counts were measured, and the final platelet concentration was adjusted to 1000×10^9/L using PPP to obtain the experimental PRP [21]. For activation, 1 mL of PRP was mixed with 0.1 mL of thrombin and 0.1 mL of calcium gluconate (final volume ratio 1:0.1:0.1) to initiate coagulation and promote growth factor release.

2.9 Treating Diabetic Ulcers in Rats With PRP

A total of 48 male rats aged 7–8 weeks and weighing 200–250 g were obtained from Hunan Saiweishi Biotechnology Co., Ltd. (Hunan, China). Thirty-six rats were randomly assigned (using a random number table) into three groups (n = 12 per group): the non-diabetic ulcer group (sham group), the diabetic ulcer group (control group), and the diabetic ulcer + PRP treatment group (PRP group). The remaining 12 rats were reserved exclusively for PRP preparation. Following successful induction of diabetic ulcers, the PRP group received 0.5 mL of PRP administered via perilesional injection on days 1, 7, 14, and 21. Rats in the sham and control groups received equivalent volumes of physiological saline. After treatment administration, wounds were covered with Vaseline gauze and sterile dressings, which were secured with adhesive tape.

Procedure for rat euthanasia by cervical dislocation (following isoflurane anesthesia):

(1) Anesthesia Induction: induce anesthesia in the rat by exposing it to 2% isoflurane delivered at a flow rate of 3 mL/min via an appropriate anesthesia system. Allow the rat to breathe the anesthetic gas for approximately 10 minutes, or until it reaches a sufficient level of surgical anesthesia (loss of righting reflex, lack of response to stimuli).

(2) Handling the rat: once adequately anesthetized, grasp the rat securely with one hand by supporting its body from the underarms and thoracic/back region. Lift the rat so that its body is suspended in the air, with the forelimbs naturally extended forward and the hind limbs hanging down.

(3) Securing the head and neck: with your other hand, use your thumb and index finger (and optionally the middle finger) to firmly but gently pinch and stabilize the rat's head and neck, specifically at the area where the head meets the cervical spine (the nape/neck base).

(4) Performing cervical dislocation: with a quick, firm, and decisive motion, apply a forward and downward force combined with a slight twisting motion to dislocate the cervical vertebrae. This action severs the spinal cord, resulting in immediate loss of consciousness and death.

(5) Confirming death: after performing cervical dislocation, carefully observe the rat for any signs of life, including breathing movements, heartbeat, or involuntary limb

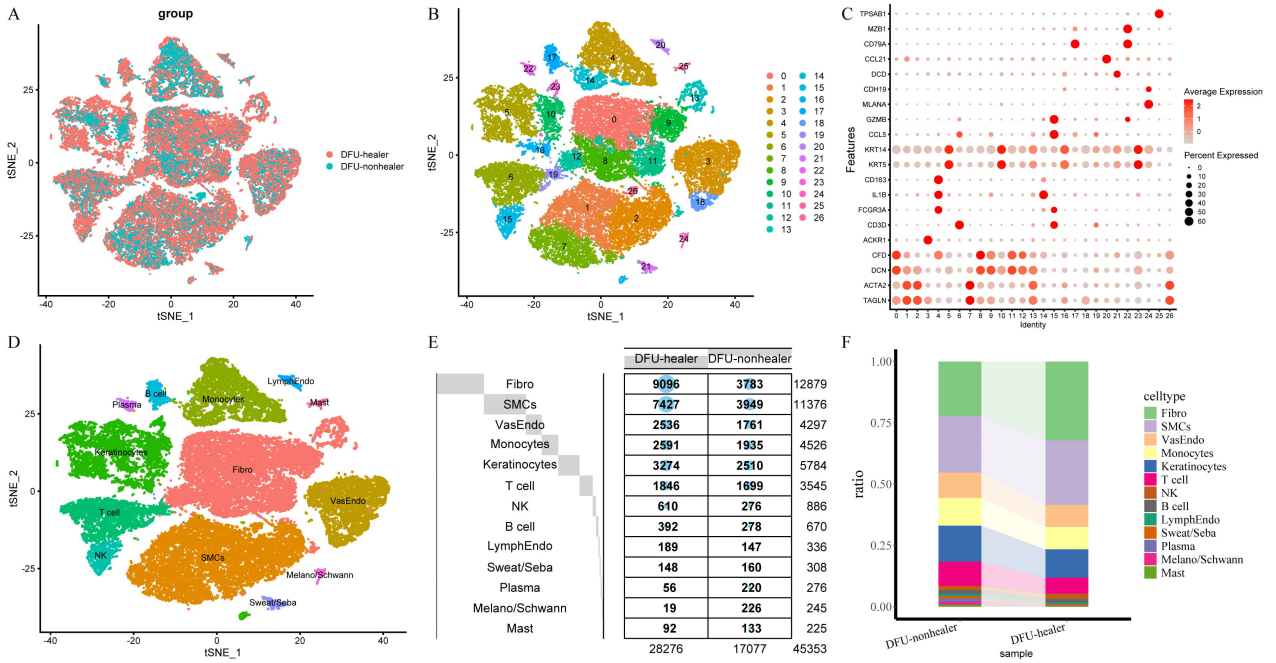

Fig. 1. Single-cell sequencing analysis of cellular heterogeneity in diabetic foot ulcers (DFU)-healer and DFU-nonhealer samples. (A,B) t-SNE–based dimensionality reduction of 45,353 cells from dataset GSE165816, identifying 27 transcriptionally distinct clusters across DFU-healer and DFU-nonhealer samples. (C) Expression patterns of canonical lineage markers across the 27 clusters. (D) Annotation of clusters into 13 major cell types based on marker gene expression. (E) Cell counts for each annotated cell type in DFU-healer and DFU-nonhealer samples. (F) Proportional distribution of the 13 cell types in DFU-healer and DFU-nonhealer groups.

movements. Absence of these signs indicates successful euthanasia.

2.10 Processing of Skin Samples

On the day of successful modeling and on day 21, wound and peri-wound tissues were excised approximately 2 mm from the wound edge. A portion of each sample was fixed in 10% neutral-buffered formalin and subsequently processed for hematoxylin–eosin (HE) staining using an HE staining kit (Beyotime, Shanghai, China). The remaining tissues collected on day 21 were transported on dry ice to Hunan Saiweishi Biotechnology Co., Ltd. (Changsha, China) for high-throughput transcriptome sequencing.

2.11 Bulk RNA Sequencing and Differential Expression Analysis of Rat Skin Tissues

Total RNA was extracted from rat skin lesions and sequenced on an Illumina platform by a commercial service provider (Hunan Saiweishi Biotechnology Co., Ltd., Changsha, China). Standard quality control procedures, including adapter trimming, read filtering, alignment to the Rattus norvegicus reference genome, and gene-level quantification (FPKM), were performed by the provider. For downstream analysis, protein-coding genes were filtered and re-analyzed in R using the edgeR–limma–voom pipeline. Differentially expressed genes were defined as those with $|\log_2 FC| > 0.8$ and $p < 0.05$ and were subsequently used for functional enrichment analyses.

3. Results

3.1 Single-Cell Sequencing Analysis of DFU Reveals Extensive Cellular Heterogeneity

Single-cell sequencing was performed on DFU-healer and DFU-nonhealer samples, and the data were visualized using tSNE for dimensionality reduction. After batch-effect correction, substantial overlap was observed between the two groups (Fig. 1A). The final analysis included 14 samples, with per-sample post-QC cell counts showing a median of 3151 (range 1764–4630; mean ≈ 3240). Median mitochondrial gene percentages (percent.mt) across samples yielded a dataset-level median of 5.61% (IQR 3.40–8.20%). DoubletFinder predicted an overall doublet rate of 4.85% (sample median 4.46%; range 0.79–9.92%), and a full QC audit is provided in **Supplementary Table 2**. A total of 27 transcriptionally distinct clusters were identified, representing diverse cellular populations within DFU tissue (Fig. 1B). Based on canonical markers, these clusters were assigned to 13 major cell types: fibroblasts (DCN+, CFD+), smooth muscle cells (TAGLN+, ACTA2+), vascular endothelial cells (ACKR1+), T cells (CD3D+), monocytes (FCGR3A+, IL1B+, CD163+), keratinocytes (KRT5+, KRT14+), NK cells (CCL5+, GZMB+), melanocytes/Schwann cells (MLANA+, CDH19+), sweat and sebaceous gland cells (DCD+), lymphatic endothelial cells (CCL21+), B cells (CD79A+), plasma cells (MZB1+), and mast

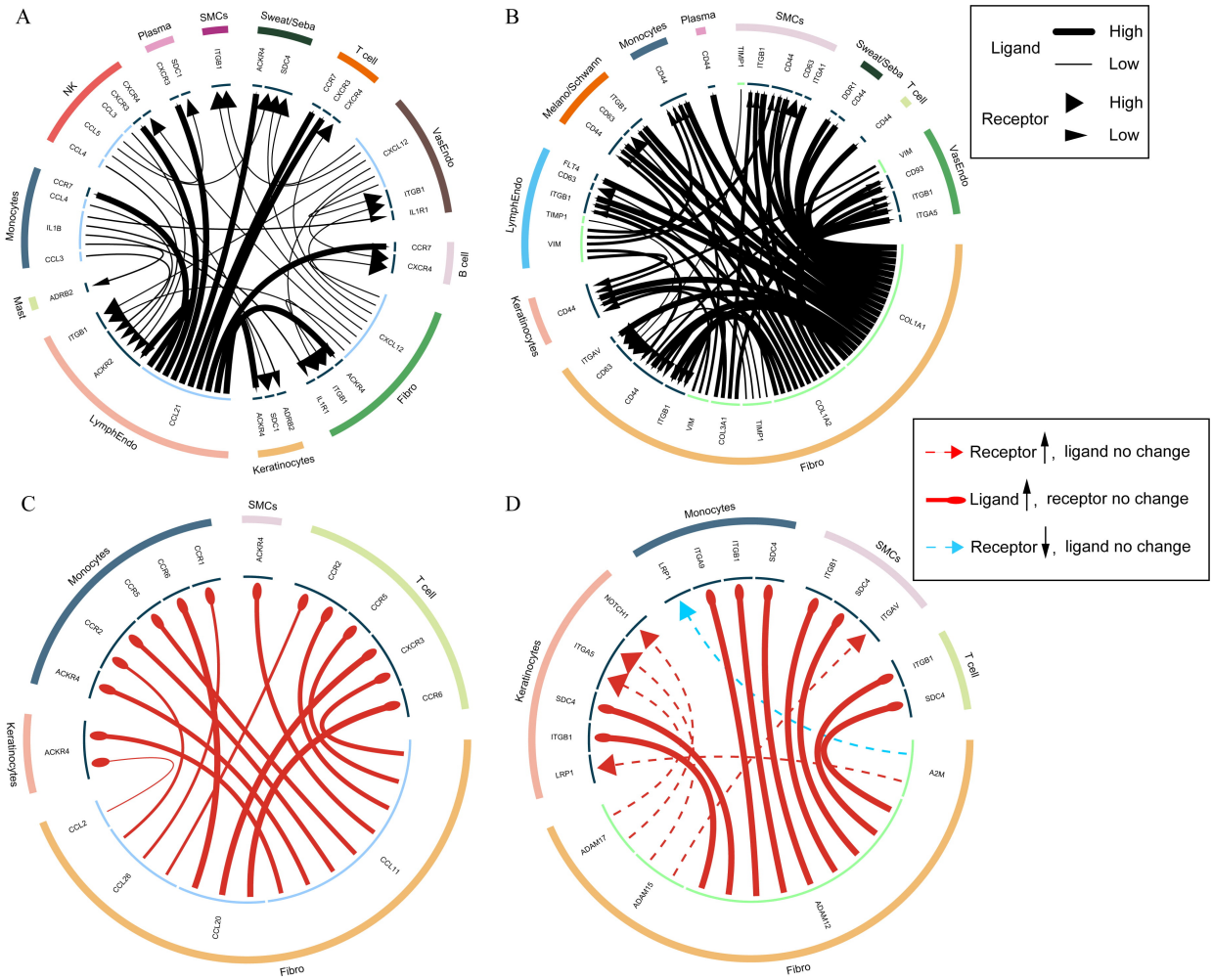

Fig. 2. Intercellular communication analysis across cell types in DFU. (A) Cytokine-mediated communication networks among cell types inferred using the iTALK package. (B) Additional ligand–receptor communication networks identified using iTALK. (C) Differential cytokine communication between fibroblasts and other cell types in DFU-healer versus DFU-nonhealer samples. (D) Differential non-cytokine communication between fibroblasts and other cell types in DFU-healer versus DFU-nonhealer samples.

cells (TPSAB1+) (Fig. 1C). **Supplementary Table 1** provides the top 20 markers per cluster, including avg_log$_2$FC, adjusted p values, and expression prevalence (pct_in_cluster/pct_other), confirming robust cluster annotation. The spatial distribution and cell-type annotation across the t-SNE map are shown in Fig. 1D. Comparison of cellular compositions revealed an increased proportion of fibroblasts in the DFU-healer group (≈32%) relative to the DFU-nonhealer group (≈25%) (Fig. 1E,F). When treating each sample as an independent unit, the mean fibroblast difference (Δ = +0.0907; +9.07 percentage points) did not reach statistical significance (Wilcoxon rank-sum p = 0.351; permutation p = 0.244; bootstrap 95% CI: –0.0253 to 0.2059). Notably, the DFU-healer group also exhibited elevated proportions of smooth muscle cells and vascular endothelial cells. Collectively, these findings suggest that specific cellular populations, particularly fibroblasts, may play key roles in driving successful DFU healing through changes in abundance and functional state.

3.2 Analysis of Cellular Communication Across Cell Types in DFU

To comprehensively characterize intercellular communication within DFU tissue, we applied the iTALK package to the scRNA-seq dataset. In the cytokine-mediated communication network, black lines denote interactions between distinct cell types, with both line and arrow thickness reflecting interaction strength. Lymphatic endothelial cells, fibroblasts, smooth muscle cells, monocytes, and T cells emerged as central hubs within this network, forming dense and highly interconnected signaling relationships (Fig. 2A). Fibroblasts also played a prominent role in additional communication networks, demonstrating strong interactions with smooth muscle cells, keratinocytes, and vascular endothelial cells (Fig. 2B). For example, fibroblast–endothelial signaling through ITGB1 is implicated in regulating angiogenesis and tissue remodeling, while fibroblast–keratinocyte interactions support wound epithelialization—an essential process for ulcer closure.

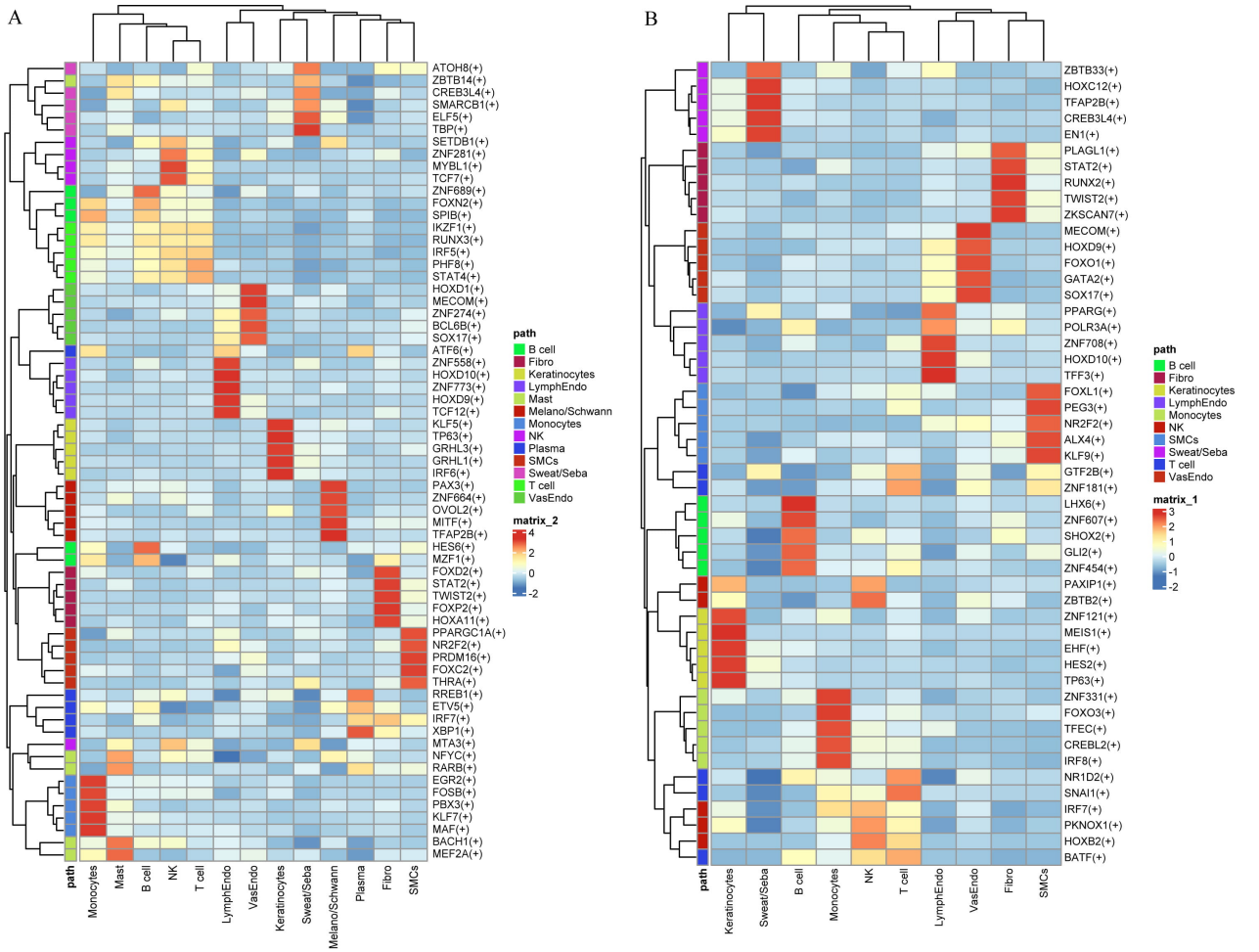

Fig. 3. Transcription factor profiling across cell types in DFU. (A) Transcription factors with high expression levels identified in each cell type from the DFU-nonhealer group. (B) Transcription factors with high expression levels identified in each cell type from the DFU-healer group.

We next compared communication patterns between DFU-healer and DFU-nonhealer samples (Fig. 2C,D). Red lines indicate cytokine interactions that were upregulated in the DFU-healer group, whereas blue lines represent downregulated interactions. Notably, fibroblast-mediated communication was markedly elevated in DFU-healer tissue, suggesting increased fibroblast activity and enhanced crosstalk with neighboring cell types. Such upregulated signaling pathways are consistent with a more pro-repair microenvironment and may contribute to improved wound healing in DFU-healer patients.

3.3 Transcription Factor Analysis Across Cell Types in DFU

To investigate gene regulatory differences between DFU-healer and DFU-nonhealer patients, we applied the SCENIC workflow to identify transcription factors (TFs) with cell type–specific regulatory activity. Distinct TF expression patterns were observed between the two groups (Fig. 3A,B). In fibroblasts from the DFU-nonhealer group, predominant TFs included FOXD2, STAT2, TWIST2, FOXP2, and HOXA11, whereas fibroblasts from the DFU-healer group were characterized by elevated expression of PLAGL1, STAT2, RUNX2, TWIST2, and ZKSCAN7. SCENIC further identified PLAGL1, RUNX2, and ZKSCAN7 as putative fibroblast-associated regulons in DFU-healers, exhibiting distinctly higher AUCell activity in fibroblasts compared with other cell types (**Supplementary Fig. 1**). Notably, these regulons were not detected by AUCell in DFU-nonhealer samples under our analysis settings. A comprehensive regulon summary, including mean AUCell values, AUCell-positive fractions, and regulon specificity scores (RSS), is provided in **Supplementary Table 3**. Analysis of differential TFs and their predicted target genes revealed significant enrichment in pathways related to NABA CORE MATRISOME and Extracellular matrix organization, indicating a strong link to fibroblast-driven matrix remodeling (Table 1). Target genes regulated by PLAGL1, RUNX2, and ZKSCAN7 showed particularly strong enrichment in these pathways, with lower p values indicating robust statistical significance. Additional associations were observed with path-

Table 1. Enrichment Analysis of target genes in FOXD2, FOXP2 and HOXA11.

GO (Gene Ontology)	Category	Description	Count	%	Log10(P)	Log10(q)
M5884	Canonical Pathways	NABA CORE MATRISOME	21	4.96	–9.4	–5.05
R-HSA-1474244	Reactome Gene Sets	Extracellular matrix organization	19	4.49	–7.25	–3.2
M5885	Canonical Pathways	NABA MATRISOME ASSOCIATED	31	7.33	–7	–3.13
GO:0002009	GO Biological Processes	Morphogenesis of an epithelium	23	5.44	–6.79	–3.05
GO:0022612	GO Biological Processes	Gland morphogenesis	11	2.6	–6.62	–2.99
GO:0060541	GO Biological Processes	Respiratory system development	15	3.55	–6.41	–2.99
R-HSA-3000178	Reactome Gene Sets	ECM proteoglycans	9	2.13	–5.94	–2.67
GO:0008283	GO Biological Processes	Cell population proliferation	27	6.38	–5.5	–2.35
R-HSA-556833	Reactome Gene Sets	Metabolism of lipids	28	6.62	–5.45	–2.34
GO:0071363	GO Biological Processes	Cellular response to growth factor stimulus	21	4.96	–5.2	–2.13
GO:0050865	GO Biological Processes	Regulation of cell activation	24	5.67	–4.96	–2.01
R-HSA-2142753	Reactome Gene Sets	Arachidonic acid metabolism	7	1.65	–4.74	–1.85
GO:0030500	GO Biological Processes	Regulation of bone mineralization	8	1.89	–4.71	–1.84

Table 2. Enrichment analysis of target genes in PLAGL1, RUNX2 and ZKSCAN7.

GO	Category	Description	Count	%	Log10(P)	Log10(q)
R-HSA-1474244	Reactome Gene Sets	Extracellular matrix organization	95	5.48	–43.98	–39.63
M5884	Canonical Pathways	NABA CORE MATRISOME	87	5.02	–40.26	–36.21
GO:0001944	GO Biological Processes	Vasculature development	100	5.77	–24.53	–20.97
GO:0097435	GO Biological Processes	Supramolecular fiber organization	104	6	–24.08	–20.64
GO:0001501	GO Biological Processes	Skeletal system development	89	5.13	–21	–17.7
R-HSA-3781865	Reactome Gene Sets	Diseases of glycosylation	44	2.54	–19.97	–16.74
R-HSA-5653656	Reactome Gene Sets	Vesicle-mediated transport	103	5.94	–19.22	–16.05
R-HSA-3000178	Reactome Gene Sets	ECM proteoglycans	31	1.79	–18.43	–15.29
GO:0001503	GO Biological Processes	Ossification	60	3.46	–17.97	–14.88
GO:0048598	GO Biological Processes	Embryonic morphogenesis	91	5.25	–17.4	–14.4
GO:0009100	GO Biological Processes	Glycoprotein metabolic process	64	3.69	–17.01	–14.08
GO:2000147	GO Biological Processes	Positive regulation of cell motility	92	5.31	–16.94	–14.02

ways involved in vasculature development and supramolecular fiber organization (Table 2), highlighting the broad regulatory influence of these TFs in promoting tissue repair and structural remodeling.

3.4 Single-Cell Transcriptome Analysis of Fibroblasts in DFU

To characterize transcriptional and functional differences between fibroblasts from DFU-healer and DFU-nonhealer samples, we performed focused analysis of fibroblast populations within the scRNA-seq dataset. After isolating fibroblasts, t-SNE dimensionality reduction identified 22 transcriptionally distinct clusters (Fig. 4A). Fibroblasts from DFU-healers (red) and DFU-nonhealers (blue) displayed clearly segregated spatial distributions (Fig. 4B), indicative of substantial differences in gene expression states and cellular functions. This divergence suggests that healing-associated fibroblasts may activate distinct regulatory programs that support wound repair. Differential expression analysis using the FindMarkers function revealed robust transcriptional differences between the two groups, which are summarized in a heatmap (Fig. 4C,D). A full list of DEGs, including $\log_2$ fold-change values, adjusted p values, and expression frequencies, is provided in **Supplementary Table 4**. Gene Set Enrichment Analysis (GSEA) demonstrated that genes upregulated in DFU-healer fibroblasts were significantly enriched in pathways related to Extracellular matrix organization and Collagen formation, highlighting their enhanced role in matrix deposition and tissue reconstruction during ulcer healing.

3.5 Pseudotime Analysis of Fibroblasts in DFU

To elucidate fibroblast state transitions during DFU healing, we performed pseudotime trajectory reconstruction using Monocle2. The resulting trajectory revealed a continuum of dynamic transcriptional changes across fibroblast states (Fig. 5A). The trajectory was rooted in a homeostatic/quiescent fibroblast subset characterized by high *DCN*, *COL1A1*/*COL1A2*, and *PDGFRA* expression and low *ACTA2* and *TAGLN* expression, positioned at a terminal tip of the learned graph (root_state = 9). From this starting point, fibroblasts progressed toward more activated, myofibroblast-like phenotypes. Fibroblast distributions along pseudotime differed markedly between groups (Fig. 5B). DFU-healer samples showed a greater abundance of fibroblasts in States 1–4, suggesting enrichment of pro-

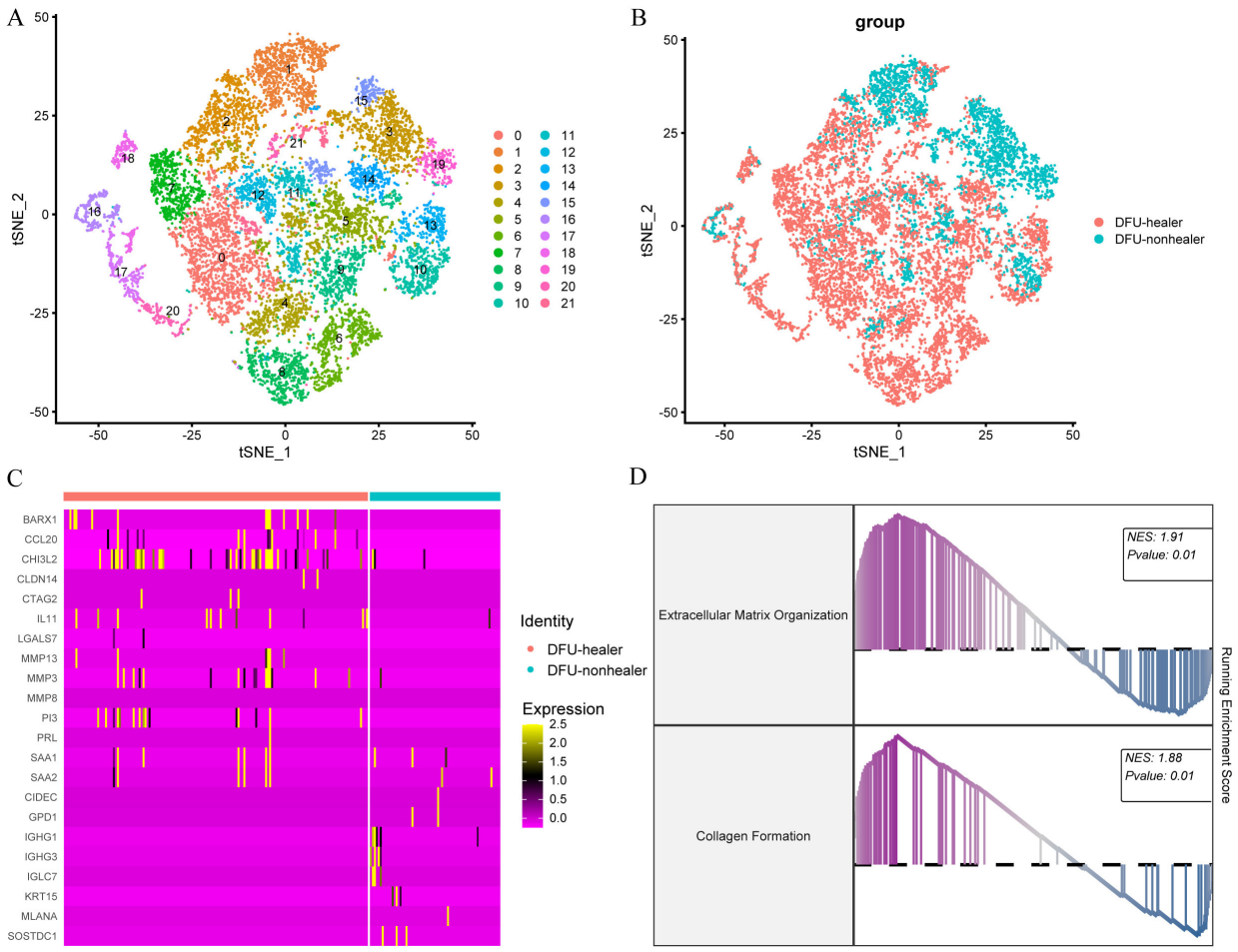

Fig. 4. Single-cell transcriptomic analysis of fibroblasts in DFU-healer and DFU-nonhealer samples. (A,B) t-SNE–based dimensionality reduction of fibroblasts, identifying 22 transcriptionally distinct clusters across DFU-healer and DFU-nonhealer groups. (C) Heatmap showing differentially expressed genes with high expression in fibroblasts from DFU-healer and DFU-nonhealer samples. (D) Gene Set Enrichment Analysis (GSEA) of differentially expressed genes between DFU-healer and DFU-nonhealer fibroblasts, highlighting enriched biological pathways.

repair fibroblast states in healing tissue. To probe the underlying regulatory mechanisms, we examined branch point 3 (branch_point = 3) and identified DEGs distinguishing the pre-branch population (State 9) from the two major fates, cell fate 1 (States 1–5) and cell fate 2 (States 6–8). These DEGs were grouped into six distinct clusters (Fig. 5C), with Clusters 1 and 5 showing elevated expression in cell fate 1, consistent with a pro-healing fibroblast trajectory. Genes from these clusters were used to construct a protein–protein interaction network in STRING (Fig. 5D). Subsequent module detection using the MCODE plugin identified key functional submodules (Fig. 5E). Enrichment analysis demonstrated that genes within these modules participated in biological processes central to tissue repair, including Collagen biosynthetic process, Platelet-derived growth factor binding, Extracellular matrix structural constituent, and Collagen type I trimer (Table 3), underscoring the importance of ECM remodeling and growth factor signaling in fibroblast-mediated DFU healing.

3.6 Histological Evaluation of the Healing Effects of PRP in a Diabetic Ulcer Rat Model

Given that several pathways enriched in key gene modules were associated with platelet activity, and prior studies have demonstrated the therapeutic potential of PRP in diabetic ulcers, we conducted histological analyses to further evaluate the impact of PRP on ulcer healing in a rat model. HE-stained tissue sections from the control, PRP-treated, and sham groups were examined on day 0 and day 21. On day 0, both the diabetic control and PRP-treated groups exhibited comparable pathological features, including compensatory epidermal thickening, marked disruption of epidermal and dermal architecture, and extensive inflammatory cell infiltration. In contrast, the non-diabetic sham group displayed noticeably milder tissue damage and reduced inflammatory infiltration (Fig. 6A–C). By day 21, the control group continued to show substantial architectural destruction and persistent inflammatory cell accumulation, indicative of poor healing. In comparison, both the PRP

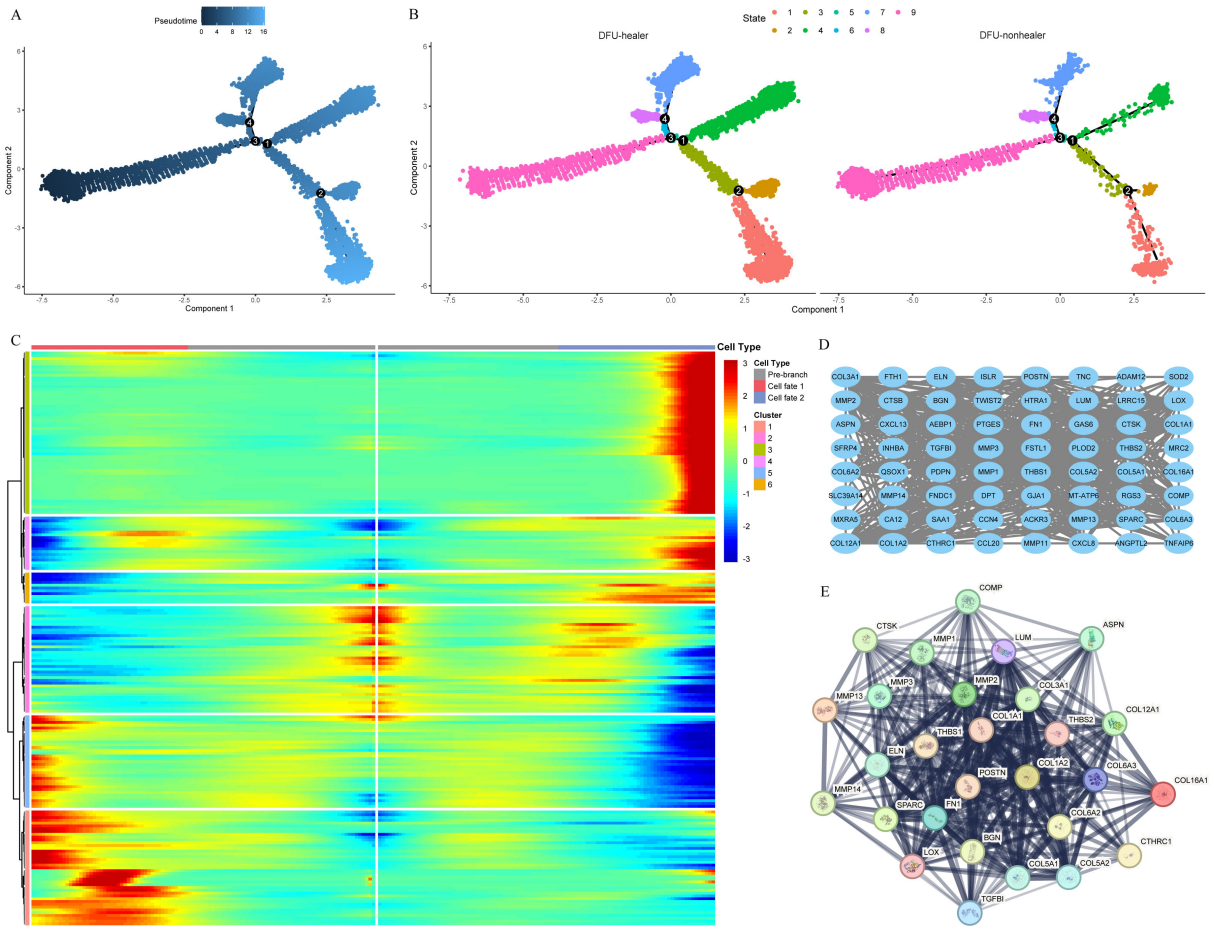

Fig. 5. Pseudotime trajectory analysis of fibroblasts. (A) Pseudotime trajectory and branching structure of fibroblasts. The color gradient from dark to light represents progression along pseudotime, with the darkest color indicating the earliest state. (B) Distribution of fibroblast states in DFU-healer and DFU-nonhealer samples along the pseudotime trajectory. (C) Heatmap of differentially expressed genes distinguishing the pre-branch population, cell fate 1, and cell fate 2. (D) Protein–protein interaction (PPI) network constructed from genes in Clusters 1 and 5. (E) Key functional modules identified within the PPI network.

and sham groups demonstrated pronounced restoration of epidermal and dermal structures, significant ulcer area reduction, active tissue regeneration, and a marked decrease in inflammatory infiltrates (Fig. 6D–F). These findings support the beneficial effects of PRP in promoting structural repair and attenuating inflammation in diabetic ulcer wounds.

3.7 Transcriptome Sequencing Analysis of Skin Lesion Tissues From Various Groups

Transcriptome sequencing and downstream bioinformatics analyses were performed on skin tissues collected from the different wound and wound-healing groups. GSEA of differentially expressed genes between the sham and control groups revealed significant enrichment in pathways such as Collagen formation, Collagen degradation, and Chemokine receptors bind chemokines (Fig. 7A), reflecting the greater structural integrity and immunological homeostasis of non-diabetic skin. A similar enrichment pattern was observed when comparing the PRP and control groups (Fig. 7B), suggesting that PRP treatment partially restores the molecular landscape of diabetic ulcers toward a non-diabetic phenotype.

To further delineate the biological functions of these genes, GO enrichment analysis was conducted across biological process (BP), cellular component (CC), and molecular function (MF) categories. In the sham versus control comparison, BP terms (Fig. 7C) were predominantly associated with leukocyte migration, extracellular matrix (ECM) organization, inflammatory response, and cell proliferation, processes essential for maintaining normal skin repair and immune defense. CC analysis (Fig. 7E) indicated enrichment in ECM structures, collagen fibers, and cell adhesion complexes, consistent with preserved tissue architecture in the sham group. MF terms (Fig. 7G) included pattern recognition receptor activity, glycosaminoglycan binding, and structural molecule activity, underscoring the functional and immunological robustness of non-diabetic skin.

In the PRP versus control comparison, BP terms (Fig. 7D) highlighted leukocyte migration, ECM remodeling, collagen degradation, and redox regulation. CC en-

Table 3. Enrichment analysis of the key module.

GO term	Description	Count in network	Strength	False discovery rate
BP GO:1903225	Negative regulation of endodermal cell differentiation	2 of 3	2.67	0.0047
BP GO:0001957	Intramembranous ossification	3 of 7	2.48	0.00014
BP GO:1902617	Response to fluoride	2 of 5	2.45	0.0091
BP GO:0035989	Tendon development	2 of 5	2.45	0.0091
BP GO:0032914	Positive regulation of transforming growth factor beta1 production	2 of 7	2.3	0.0145
BP GO:0071492	Cellular response to UV-A	3 of 11	2.28	0.00034
BP GO:0060346	Bone trabecula formation	2 of 8	2.25	0.017
BP GO:0033622	Integrin activation	2 of 10	2.15	0.0217
BP GO:0032964	Collagen biosynthetic process	2 of 10	2.15	0.0217
MF GO:0048407	Platelet-derived growth factor binding	4 of 11	2.41	2.70×10^{-6}
MF GO:0030020	Extracellular matrix structural constituent conferring tensile strength	9 of 28	2.35	1.11×10^{-15}
MF GO:005518	Collagen binding	11 of 66	2.07	7.63×10^{-17}
MF GO:0043394	Proteoglycan binding	5 of 37	1.98	2.28×10^{-6}
MF GO:0005201	Extracellular matrix structural constituent	16 of 131	1.93	5.43×10^{-24}
MF GO:0001968	Fibronectin binding	3 of 30	1.85	0.0029
MF GO:0050840	Extracellular matrix binding	5 of 56	1.8	1.22×10^{-5}
MF GO:0005178	Integrin binding	8 of 159	1.55	4.93×10^{-8}
MF GO:0004222	Metalloendopeptidase activity	5 of 114	1.49	0.0002
CC GO:000584	Collagen type I trimer	2 of 2	2.85	0.0013
CC GO:000588	Collagen type V trimer	3 of 4	2.72	1.52×10^{-5}
CC GO:000583	Fibrillar collagen trimer	7 of 12	2.61	7.49×10^{-14}
CC GO:000592	Collagen type XI trimer	2 of 5	2.45	0.0042
CC GO:000593	FACIT collagen trimer	2 of 6	2.37	0.0053
CC GO:000577	Fibrinogen complex	2 of 8	2.25	0.0077
CC GO:000581	Collagen trimer	13 of 95	1.98	3.37×10^{-20}
CC GO:0062023	Collagen-containing extracellular matrix	23 of 407	1.6	2.05×10^{-31}
CC GO:0031012	Extracellular matrix	27 of 552	1.54	1.30×10^{-37}

richment (Fig. 7F) emphasized localization to ECM components, collagen fibers, and membrane-associated proteins, while MF terms (Fig. 7H) included pattern recognition receptor activity, structural molecule activity, and redox enzyme activity. Together, these results suggest that PRP enhances ECM integrity and modulates immune and metabolic pathways to promote wound repair, thereby shifting diabetic ulcer gene expression profiles toward a healthier state.

Differential expression analysis further identified highly expressed genes across three comparisons: sham versus control, PRP versus control, and DFU-healer versus DFU-nonhealer fibroblasts (Fig. 8A). Venn analysis revealed 26 overlapping genes shared among all comparisons. Heatmap visualization (Fig. 8B) demonstrated high expression of these genes in the sham group, pronounced downregulation in the control group, and partial restoration in PRP-treated tissue, approaching levels observed in non-diabetic skin. This pattern indicates that PRP partially normalizes expression of genes associated with skin repair and immune regulation in diabetic wounds. Enrichment analysis (Fig. 8C) showed that these 26 genes were significantly associated with pathways such as Extracellular matrix organization, regulation of phagocytosis, and regulation of actin filament polymerization, highlighting their central roles in tissue remodeling, cytoskeletal dynamics, and immune processes relevant to DFU healing and PRP's mechanism of action.

4. Discussion

Diabetic ulcers are among the most common chronic wounds and, when left untreated, markedly increase the risk of bacterial infection [22]. As highlighted by Dr. Chandan K. Sen, diabetic ulcers also impose the second-highest economic burden among chronic wound types, surpassed only by surgical wounds [23], placing substantial financial strain on both individuals and healthcare systems [24]. PRP, which contains a platelet concentration approximately fivefold higher than baseline levels [25], provides a rich source of growth factors that support soft-tissue regeneration. Beyond its relevance to diabetic ulcers, PRP has demonstrated therapeutic benefits in diverse clinical settings, including accelerated gingival wound healing [26], reduction of osteoarthritis-related pain with potential disease-modifying effects [27], and enhanced peripheral nerve regeneration following sciatic nerve injury [28].

In this study, we combined single-cell sequencing, cell–cell communication analysis, transcription factor pro-

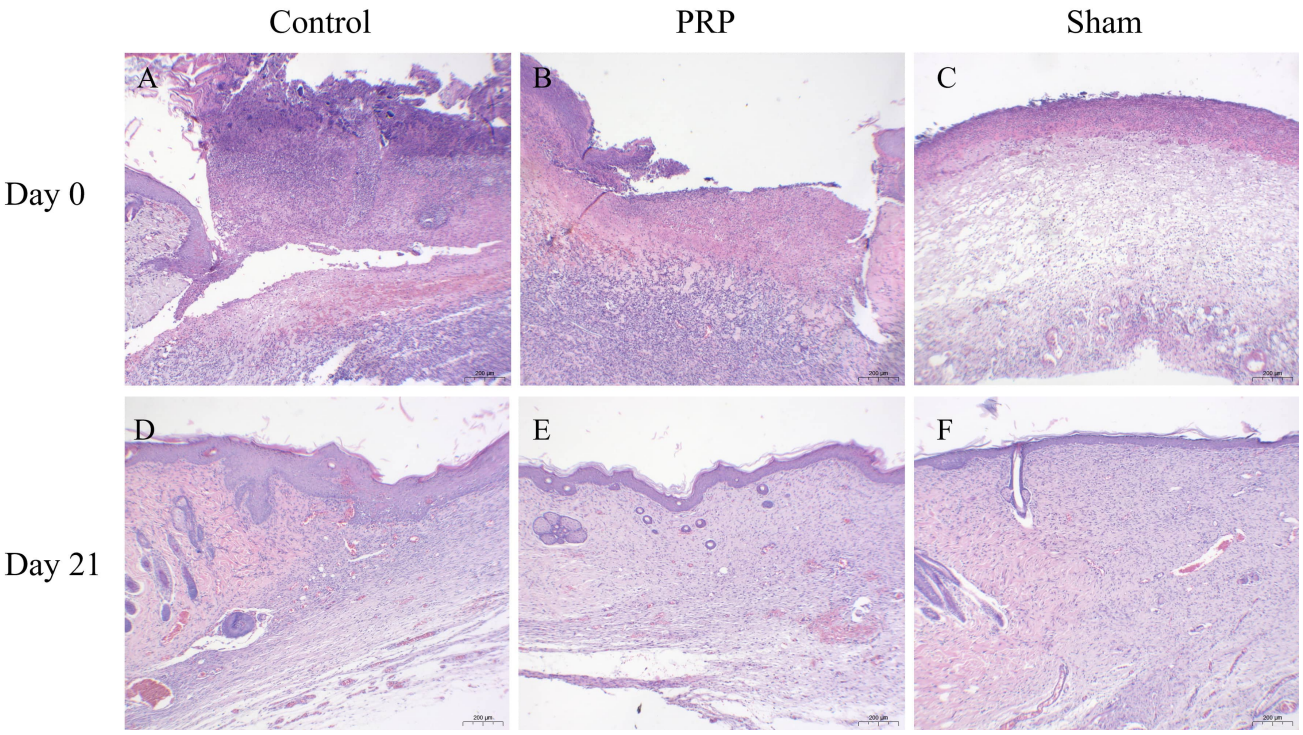

Fig. 6. Hematoxylin–eosin (HE) staining of ulcer tissue in the rat model. (A–C) HE-stained ulcer tissue from the Control, platelet-rich plasma (PRP), and Sham groups on day 0. (D–F) HE-stained ulcer tissue from the Control, PRP, and Sham groups on day 21. Scale bar = 200 μm.

filing, pseudotime reconstruction, and PRP-treated animal models to systematically investigate the role of fibroblasts in diabetic ulcer pathogenesis and repair. Single-cell analysis revealed extensive cellular heterogeneity within DFU tissues, with fibroblast abundance markedly higher in healed than in non-healed samples. Functionally, these fibroblasts contribute to tissue repair through secretion of ECM components such as collagen and fibronectin, as well as pro-angiogenic mediators that promote vascular regeneration [29,30]. Intercellular communication mapping further demonstrated that fibroblasts actively interact with smooth muscle cells, vascular endothelial cells, and keratinocytes, supporting the coordinated multicellular responses required for effective ulcer resolution [31].

Transcription factor analysis identified PLAGL1, RUNX2, and ZKSCAN7 as selectively enriched in fibroblasts from healed tissue, regulating gene programs associated with ECM organization, angiogenesis, and cell migration, hallmarks of active wound repair. Pseudotime analysis provided additional insight by delineating the temporal emergence of pro-healing fibroblast subpopulations, underscoring their central role in orchestrating tissue repair dynamics. These findings establish fibroblasts as key drivers of the diabetic ulcer healing process and support PRP as a biologically rational therapeutic strategy capable of enhancing fibroblast-mediated regeneration.

Animal model experiments further confirmed the therapeutic efficacy of PRP, demonstrating accelerated ulcer closure in diabetic rats [32]. By day 21, histological analysis revealed substantial regeneration of the epidermal and dermal layers, accompanied by a marked reduction in inflammatory infiltrates in PRP-treated wounds. Transcriptomic profiling reinforced these observations: PRP-treated diabetic ulcers displayed gene expression patterns that closely resembled those of non-diabetic controls, with pronounced enrichment in pathways related to *Collagen formation* and *Extracellular matrix organization*. These results suggest that PRP promotes wound repair, at least in part, by modulating fibroblast activity and restoring ECM-related functions. Consistent with this interpretation, Venn diagram and enrichment analyses identified a set of key genes, shared across sham, PRP-treated, and DFU-healer samples, whose expression profiles were partially restored by PRP. Many of these genes are central to ECM organization and cell migration, processes typically impaired in diabetic wounds. Together, these findings provide mechanistic validation for PRP's role in re-establishing tissue homeostasis and enhancing fibroblast-driven repair.

Although this integrated study provides compelling evidence for the central role of fibroblasts in diabetic ulcer healing and demonstrates the therapeutic potential of PRP, several limitations should be considered when interpreting the findings and designing future research. (1) Preclinical model constraints: The primary evidence is derived from an STZ-induced diabetic rat model. Although widely used, this model predominantly reflects type 1 diabetes and may

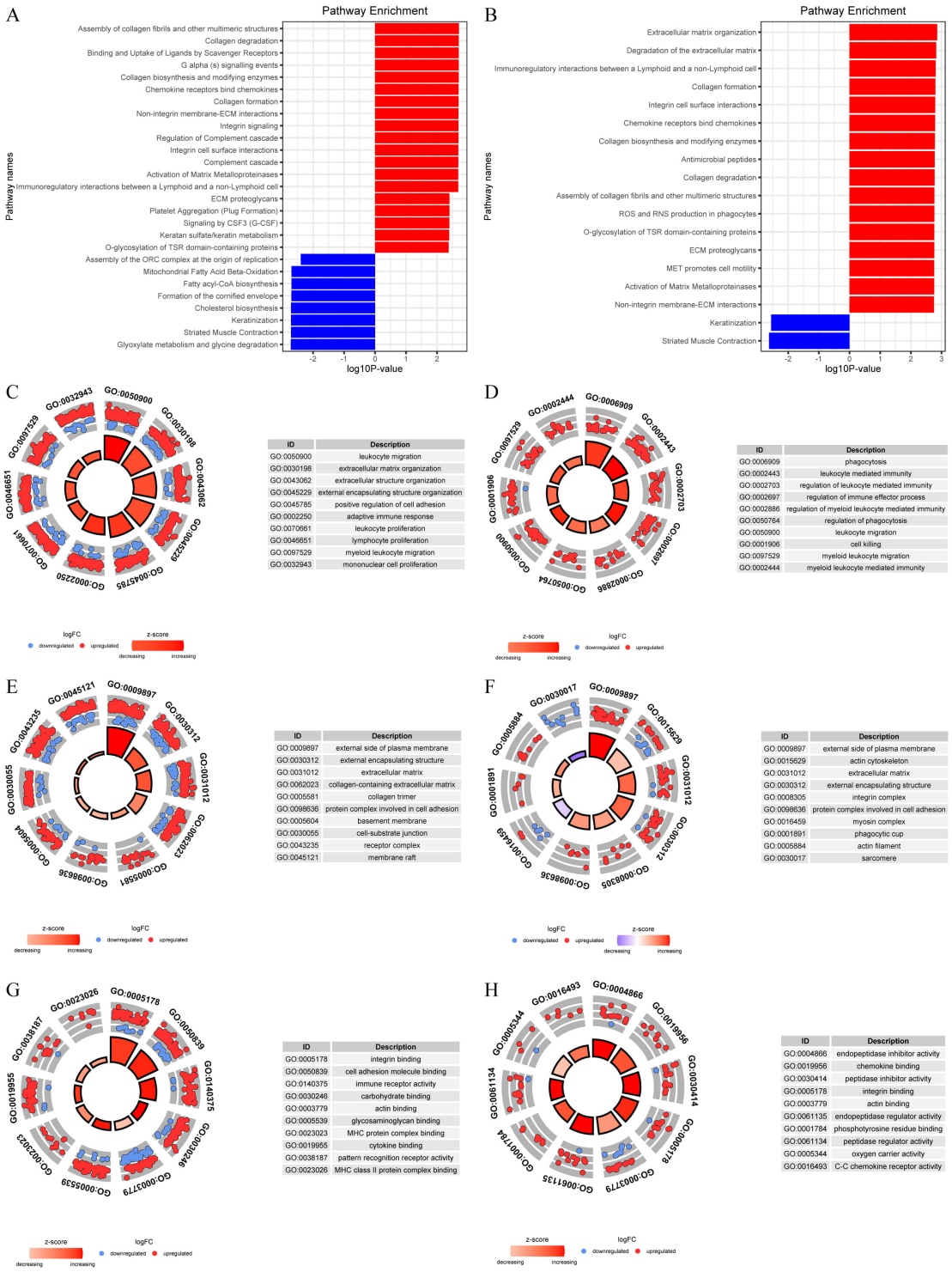

Fig. 7. Enrichment analysis of highly expressed genes in sham, PRP, and control groups. (A) GSEA of differentially expressed genes between the Sham and Control groups. (B) GSEA of differentially expressed genes between the PRP and Control groups. (C) GO biological process (BP) enrichment of differentially expressed genes between the Sham and Control groups. (D) GO BP enrichment of differentially expressed genes between the PRP and Control groups. (E) GO cellular component (CC) enrichment of differentially expressed genes between the Sham and Control groups. (F) GO CC enrichment of differentially expressed genes between the PRP and Control groups. (G) GO molecular function (MF) enrichment of differentially expressed genes between the Sham and Control groups. (H) GO MF enrichment of differentially expressed genes between the PRP and Control groups.

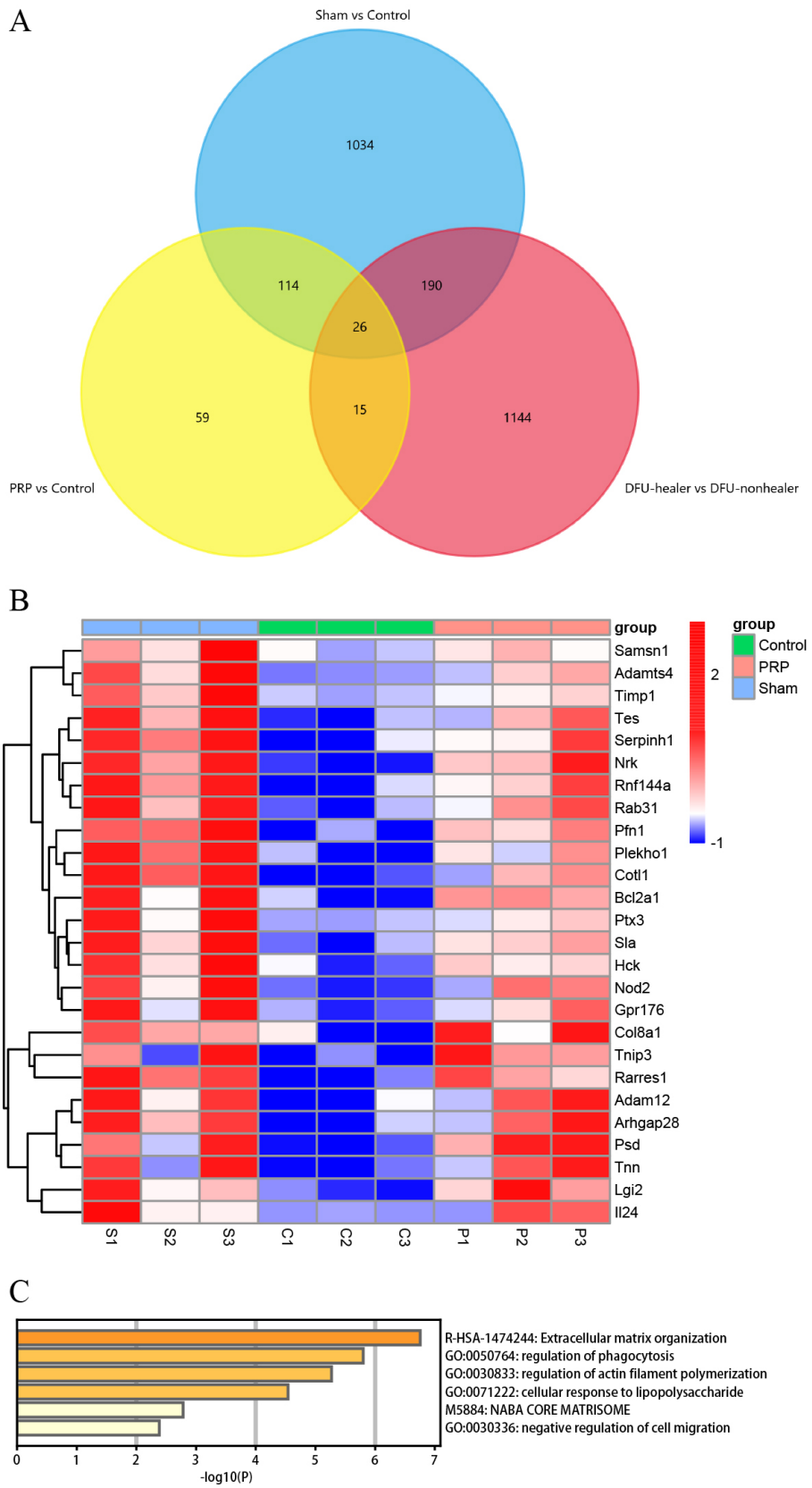

Fig. 8. Differentially expressed fibroblast-associated genes and their functional enrichment. (A) Venn diagram identifying overlapping fibroblast-related differentially expressed genes across comparisons. (B) Heatmap showing the expression patterns of key overlapping genes in the Sham, Control, and PRP groups. (C) Functional enrichment analysis of the key overlapping genes.

not fully capture the metabolic complexity of type 2 diabetes, which accounts for most clinical cases of diabetic ulcers. In addition, the controlled wound environment in rodents differs substantially from the chronic, polymicrobial, pressure-prone conditions characteristic of human ulcers. Therefore, validation in well-designed human clinical cohorts is necessary to establish translational relevance. (2) Sample size and statistical power: The manuscript does not report the number of animals per experimental group, and no a priori power analysis was performed. Although group sizes were informed by prior studies, the absence of formal power calculations limits our ability to assess the risk of Type II error. As this study was exploratory and mechanistically focused, future confirmatory studies should incorporate power analyses to ensure sufficient sample sizes for detecting biologically meaningful effects. (3) Narrowed cellular focus: Our analysis deliberately concentrated on fibroblast heterogeneity and function. While this yielded in-depth insights, it limited broader interpretation. Other key cell types involved in wound repair, such as macrophages, endothelial progenitor cells, and keratinocytes, were not comprehensively examined. A more integrative, multicellular analysis will be essential to fully elucidate the cellular crosstalk governing DFU healing and the mechanisms underlying PRP efficacy. (4) Mechanistic validation gap: Although our multi-omics findings strongly associate PLAGL1, RUNX2, and ZKSCAN7 with a pro-healing fibroblast phenotype, these correlative results do not establish causality. Definitive validation of these transcription factors as regulators of fibroblast fate will require *in vivo* functional studies, such as fibroblast-specific knockout or knockdown models. Such approaches will be necessary to confirm causal roles and assess their potential as therapeutic targets. (5) Lack of PRP standardization: A major challenge in translating PRP therapy lies in the absence of standardized preparation protocols. Like many studies, ours defined PRP primarily by platelet count; however, critical parameters, including concentrations and bioactivity of growth factors (e.g., PDGF, VEGF), leukocyte content, and activation methods, were not standardized and may influence therapeutic response. Future research must work toward consensus on PRP preparation to ensure reproducibility and enable meaningful comparisons across studies. (6) Absence of external validation for the 26-gene signature: The fibroblast-related 26-gene "core" signature identified in this study was derived solely from the integrated dataset analyzed here (Section 3.7; Fig. 8). Due to the lack of an independent DFU scRNA-seq or bulk-transcriptomic cohort with compatible outcome data, we could not assess its diagnostic or prognostic performance through external validation. Thus, this gene set should be viewed as hypothesis-generating, and future studies involving independent patient cohorts will be required to evaluate and refine its clinical utility. Addressing these limitations through human validation, rigorous study design, broader cellular profiling, direct functional experiments, and standardized PRP preparation will be essential to advance these findings toward clinical translation.

5. Conclusion

This integrated study highlights the pivotal role of fibroblast functional dynamics in diabetic ulcer repair. Single-cell transcriptomic analysis demonstrated a marked expansion of fibroblast populations in healed DFU tissue (32%) compared with non-healed counterparts (25%). These healing-associated fibroblasts exhibited enhanced ECM synthesis and collagen formation, driven by three key transcription factors, PLAGL1, RUNX2, and ZKSCAN7, that regulate pathways involved in angiogenesis and cell migration. Importantly, our findings confirm PRP as a potent modulator of fibroblast-mediated reparative processes. PRP not only promoted fibroblast proliferation and functional activation but also accelerated ulcer resolution through reduced inflammation and improved ECM remodeling. Collectively, these results underscore fibroblasts as central effectors of diabetic ulcer healing and support PRP as a promising translational therapeutic strategy. Future studies should focus on optimizing PRP preparation protocols and evaluating combination approaches to further enhance clinical outcomes for patients with diabetic ulcers.

Availability of Data and Materials

The datasets generated and analyzed during the current study have been deposited in the GEO database under accession number GSE280992. The datasets used and analyzed during the current study are available from the corresponding author on reasonable request.

Author Contributions

XJL, ZHH and CYL: conception and experimental design, experimental performing, collection and analysis of data, writing of the manuscript. MLC and LZZ: experimental performing, collection and analysis of data, writing of the manuscript. ZJL and JT: experimental performing, collection and analysis of data, writing of the manuscript assisting in revising the manuscript. All authors contributed to editorial changes in the manuscript. All authors read and approved the final manuscript. All authors have participated sufficiently in the work and agreed to be accountable for all aspects of the work.

Ethics Approval and Consent to Participate

All animal experiments were conducted in a humane manner. Experimental procedures were approved by the Animal Care and Use Committee of Zhongshan City People's Hospital (Ethics Approval No. K2023-072) and were performed in accordance with the Guidelines for the Care and Use of Laboratory Animals published by the National Academies Press.

Acknowledgment

Thanks to Hunan Saiweishi Biotechnology Co., Ltd. (Changsha, China) for their technical support and consultation.

Funding

This work was supported by Guangdong Provincial Administration of Traditional Chinese Medicine (grant number 20241357).

Conflict of Interest

All authors declare no conflicts of interest. Despite they received technical support and consultation from Hunan Saiweishi Biotechnology Co., Ltd., the judgments in data interpretation and writing were not influenced by this relationship.

Supplementary Material

Supplementary material associated with this article can be found, in the online version, at https://doi.org/10.31083/FBL47450.

References

[1] Yoo HJ, Hong CO, Ha SK, Lee KW. Chebulic Acid Prevents Methylglyoxal-Induced Mitochondrial Dysfunction in INS-1 Pancreatic β-Cells. Antioxidants. 2020; 9: 771. https://doi.org/10.3390/antiox9090771.

[2] Doğruel H, Aydemir M, Balci MK. Management of diabetic foot ulcers and the challenging points: An endocrine view. World Journal of Diabetes. 2022; 13: 27–36. https://doi.org/10.4239/wjd.v13.i1.27.

[3] Jnana A, Muthuraman V, Varghese VK, Chakrabarty S, Murali TS, Ramachandra L, *et al*. Microbial Community Distribution and Core Microbiome in Successive Wound Grades of Individuals with Diabetic Foot Ulcers. Applied and Environmental Microbiology. 2020; 86: e02608-19. https://doi.org/10.1128/AEM.02608-19.

[4] Vas P, Rayman G, Dhatariya K, Driver V, Hartemann A, Londahl M, *et al*. Effectiveness of interventions to enhance healing of chronic foot ulcers in diabetes: a systematic review. Diabetes/metabolism Research and Reviews. 2020; 36: e3284. https://doi.org/10.1002/dmrr.3284.

[5] Yang F, Chen E, Yang Y, Han F, Han S, Wu G, *et al*. The Akt/FoxO/p27^{Kip1} axis contributes to the anti-proliferation of pentoxifylline in hypertrophic scars. Journal of Cellular and Molecular Medicine. 2019; 23: 6164–6172. https://doi.org/10.1111/jcmm.14498.

[6] Barman SR, Chan SW, Kao FC, Ho HY, Khan I, Pal A, *et al*. A self-powered multifunctional dressing for active infection prevention and accelerated wound healing. Science Advances. 2023; 9: eadc8758. https://doi.org/10.1126/sciadv.adc8758.

[7] Greene CJ, Anderson S, Barthels D, Howlader MSI, Kanji S, Sarkar J, *et al*. DPSC Products Accelerate Wound Healing in Diabetic Mice through Induction of SMAD Molecules. Cells. 2022; 11: 2409. https://doi.org/10.3390/cells11152409.

[8] Watson ER, Mora A, Taherian Fard A, Mar JC. How does the structure of data impact cell-cell similarity? Evaluating how structural properties influence the performance of proximity metrics in single cell RNA-seq data. Briefings in Bioinformatics. 2022; 23: bbac387. https://doi.org/10.1093/bib/bbac387.

[9] Wang Z, Wei D, Li S, Tang Q, Lu G, Gu S, *et al*. Healing mechanism of diabetic foot ulcers using single-cell RNA-sequencing. Annals of Translational Medicine. 2023; 11: 210. https://doi.org/10.21037/atm-23-240.

[10] Smith OJ, Kanapathy M, Khajuria A, Prokopenko M, Hachach-Haram N, Mann H, *et al*. Protocol for a systematic review of the efficacy of fat grafting and platelet-rich plasma for wound healing. Systematic Reviews. 2017; 6: 111. https://doi.org/10.1186/s13643-017-0505-8.

[11] Wang ZQ, Lai QW, Gao X, Wu QY, Dong TT, Tsim KW. Platelet-Rich Plasma Extract Derived from Animals Shows Potential in Promoting Wound Healing and Suppressing Inflammatory Response in Skin Cells. Cells. 2025; 14: 526. https://doi.org/10.3390/cells14070526.

[12] Xu P, Wu Y, Zhou L, Yang Z, Zhang X, Hu X, *et al*. Platelet-rich plasma accelerates skin wound healing by promoting re-epithelialization. Burns & Trauma. 2020; 8: tkaa028. https://doi.org/10.1093/burnst/tkaa028.

[13] Misiura M, Guszczyn T, Oscilowska I, Baszanowska W, Palka J, Miltyk W. Platelet-Rich Plasma Promotes the Proliferation of Human Keratinocytes via a Progression of the Cell Cycle. A Role of Prolidase. International Journal of Molecular Sciences. 2021; 22: 936. https://doi.org/10.3390/ijms22020936.

[14] Theocharidis G, Thomas BE, Sarkar D, Mumme HL, Pilcher WJR, Dwivedi B, *et al*. Single cell transcriptomic landscape of diabetic foot ulcers. Nature Communications. 2022; 13: 181. https://doi.org/10.1038/s41467-021-27801-8.

[15] Butler A, Hoffman P, Smibert P, Papalexi E, Satija R. Integrating single-cell transcriptomic data across different conditions, technologies, and species. Nature Biotechnology. 2018; 36: 411–420. https://doi.org/10.1038/nbt.4096.

[16] Korsunsky I, Millard N, Fan J, Slowikowski K, Zhang F, Wei K, *et al*. Fast, sensitive and accurate integration of single-cell data with Harmony. Nature Methods. 2019; 16: 1289–1296. https://doi.org/10.1038/s41592-019-0619-0.

[17] Aibar S, González-Blas CB, Moerman T, Huynh-Thu VA, Imrichova H, Hulselmans G, *et al*. SCENIC: single-cell regulatory network inference and clustering. Nature Methods. 2017; 14: 1083–1086. https://doi.org/10.1038/nmeth.4463.

[18] Yu G, Wang LG, Han Y, He QY. clusterProfiler: an R package for comparing biological themes among gene clusters. Omics. 2012; 16: 284–287. https://doi.org/10.1089/omi.2011.0118.

[19] Qiu X, Mao Q, Tang Y, Wang L, Chawla R, Pliner HA, *et al*. Reversed graph embedding resolves complex single-cell trajectories. Nature Methods. 2017; 14: 979–982. https://doi.org/10.1038/nmeth.4402.

[20] Lau TW, Sahota DS, Lau CH, Chan CM, Lam FC, Ho YY, *et al*. An in vivo investigation on the wound-healing effect of two medicinal herbs using an animal model with foot ulcer. European Surgical Research. 2008; 41: 15–23. https://doi.org/10.1159/000122834.

[21] Tian J, Cheng LHH, Cui X, Lei XX, Tang JB, Cheng B. Application of standardized platelet-rich plasma in elderly patients with complex wounds. Wound Repair and Regeneration. 2019; 27: 268–276. https://doi.org/10.1111/wrr.12702.

[22] Tsegay F, Elsherif M, Butt H. Smart 3D Printed Hydrogel Skin Wound Bandages: A Review. Polymers. 2022; 14: 1012. https://doi.org/10.3390/polym14051012.

[23] Sen CK. Human Wounds and Its Burden: An Updated Compendium of Estimates. Advances in Wound Care. 2019; 8: 39–48. https://doi.org/10.1089/wound.2019.0946.

[24] Raghav A, Khan ZA, Labala RK, Ahmad J, Noor S, Mishra BK. Financial burden of diabetic foot ulcers to world: a progressive topic to discuss always. Therapeutic Advances in Endocrinology and Metabolism. 2018; 9: 29–31. https://doi.org/10.1177/2042018817744513.

[25] Ricci E, Riva G, Dagna F, Cavalot AL. The use of platelet-rich

plasma gel in superficial parotidectomy. Acta Otorhinolaryngologica Italica. 2019; 39: 363–366. https://doi.org/10.14639/0392-100X-2093.

[26] Samani MK, Saberi BV, Ali Tabatabaei SM, Moghadam MG. The clinical evaluation of platelet-rich plasma on free gingival graft's donor site wound healing. European Journal of Dentistry. 2017; 11: 447–454. https://doi.org/10.4103/ejd.ejd_76_17.

[27] Gupta A. Platelet-Rich Plasma One Week Prior to Hyaluronic Acid vs. Platelet-Rich Plasma Alone for the Treatment of Knee Osteoarthritis. Biomedicines. 2022; 10: 2805. https://doi.org/10.3390/biomedicines10112805.

[28] Wang SL, Liu XL, Kang ZC, Wang YS. Platelet-rich plasma promotes peripheral nerve regeneration after sciatic nerve injury. Neural Regeneration Research. 2023; 18: 375–381. https://doi.org/10.4103/1673-5374.346461.

[29] Hu W, Shi J, Lv W, Jia X, Ariga K. Regulation of stem cell fate and function by using bioactive materials with nanoarchitectonics for regenerative medicine. Science and Technology of Advanced Materials. 2022; 23: 393–412. https://doi.org/10.1080/14686996.2022.2082260.

[30] Murdock MH, Badylak SF. Biomaterials-based In Situ Tissue Engineering. Current Opinion in Biomedical Engineering. 2017; 1: 4–7. https://doi.org/10.1016/j.cobme.2017.01.001.

[31] Lucas T, Schäfer F, Müller P, Eming SA, Heckel A, Dimmeler S. Light-inducible antimiR-92a as a therapeutic strategy to promote skin repair in healing-impaired diabetic mice. Nature Communications. 2017; 8: 15162. https://doi.org/10.1038/ncomms15162.

[32] Chen L, Wu D, Zhou L, Ye Y. Platelet-rich plasma promotes diabetic ulcer repair through inhibition of ferroptosis. Annals of Translational Medicine. 2022; 10: 1121. https://doi.org/10.21037/atm-22-4654.